ELSEVIER

Biochimica et Biophysica Acta 1370 (1998) 64–76

BIOCHIMICA ET BIOPHYSICA ACTA
BBA

Phase structures of binary lipid bilayers as revealed by permeability of small molecules

Tian-Xiang Xiang, Bradley D. Anderson *

Department of Pharmaceutics and Pharmaceutical Chemistry, University of Utah, Salt Lake City, UT 84108, USA

Received 2 June 1997; revised 17 September 1997; accepted 22 September 1997

Abstract

The effects of changes in bilayer phase structure on the permeability of acetic acid and trimethylacetic acid were studied in large unilamellar vesicles (LUVs) composed of dipalmitoylphosphatidylcholine (DPPC)/cholesterol (CHOL), dihexadecylphosphatidylcholine (DHPC)/CHOL, or DPPC/dimyristoylphosphatidylcholine (DMPC) using an NMR line-broadening method. Phase transitions were induced by changes in temperature and lipid composition (i.e., X_{CHOL} was varied from 0.0 to 0.5 and X_{DMPC} from 0.0 to 1.0). In DPPC/CHOL and DHPC/CHOL bilayers, the addition of CHOL induces only a modest change in the permeability coefficient (P_m) of acetic acid in the gel-phase (P'_β) but significantly reduces P_m in ordered and disordered liquid-crystalline phases (L_o and L_α). Abrupt changes in slopes in semi-logarithmic plots of P_m vs. X_{CHOL} occur at specific values of X_{CHOL} and temperature corresponding to the boundaries between P'_β and L_o or between L_α and L_o phases. In most respects, phase diagrams generated from the break points in plots of P_m vs. X_{CHOL} obtained at various temperatures in DHPC/CHOL and DPPC/CHOL bilayers closely resemble those constructed previously for DPPC/CHOL bilayers using NMR and DSC methods. Above T_m, the phase diagrams generated from permeability data reveal the presence of both the disordered (L_α) and the ordered (L_o) liquid-crystalline phases, as well as the two-phase coexistence region. In DPPC/DMPC bilayers, the addition of DMPC increases P_m dramatically in the gel phase but only slightly in the liquid-crystalline phase. Abrupt changes in slopes in semi-logarithmic plots of P_m vs. X_{DMPC} also occur at specific values of X_{DMPC} and temperature, from which a phase diagram can be constructed which closely resembles diagrams obtained previously by other methods. These correlations indicate that trans-bilayer permeability measurements can be used to construct lipid bilayer phase diagrams. Positive deviations of P_m from predicted values based on the phase lever rule are observed in the two-phase coexistence regions with the degree of the deviation depending on bilayer chemical composition and temperature. These results may reflect a specific contribution of the interfacial region between two phases to higher solute permeability or may be due to the higher lateral compressibility of lipid bilayers in the two-phase coexistence region. © 1998 Elsevier Science B.V.

Keywords: Permeability; Phospholipid; Cholesterol; Lipid bilayer; Membrane transport; Phase diagram

1. Introduction

One of the major functions of biological membranes is to regulate the permeation of various chemical species into and out of cells. Although the transport of a large number of molecules of biological interest involves carriers and channel proteins, passive permeation across the membrane lipid bilayers driven by a chemical potential gradient occurs invariably for any chemical species and is probably the

* Corresponding author. Fax: +1 (801)-585-3614; E-mail: banderson@deans.pharm.utah.edu

PII S0005-2736(97)00244-7

predominant mechanism by which many drug molecules reach their intended sites of action.

Biological membranes are usually composed of multiple lipid constituents, in which non-ideal mixing of different lipids can cause lateral heterogeneity and the formation of a mosaic of two or more stable lipid domains of different chemical composition [1–3]. While the lipids comprising most biomembranes are in their liquid-crystalline state under physiological conditions, in some cases, such as in the stratum corneum, the lipid bilayers may be primarily in their gel state or, alternatively, liquid-crystalline and gel-state domains may coexist [4–6]. Even in fluid biomembranes, two liquid-crystalline phases may coexist [7]. In bilayer membranes containing more than one lipid component, phase segregation may result from mismatch of the hydrophobic portions [8–10] or head groups [11,12] of the constituent molecules, or may be induced by proteins [13,14] or other additives such as ethanol [15]. Lipid bilayers containing cholesterol (CHOL) may also exhibit phase separation into cholesterol-rich (liquid-ordered) and cholesterol-poor (liquid-disordered) domains with increasing cholesterol content [16–21], though the molecular organization in these systems is still a subject of debate as other structural models such as dynamic microdomains and regular hexagonal superlattices have also been proposed [22–26]. Because of their high cholesterol content, many biological membranes are likely to exist in the liquid-ordered/liquid-disordered coexistence region at 37°C [16].

Phase transitions or phase separations in bilayers are usually accompanied by sudden changes of lipid chain ordering and other physicochemical properties which have been successfully detected by NMR, ESR, fluorescence and other optical methods [7,18,21,27]. However, the fundamental role of phase structure in regulating solute permeation across lipid bilayers has rarely been addressed systematically. Clearly, the permeability properties of a lipid bilayer are not likely to depend in a regular fashion upon lipid composition over a wide range, as a bilayer membrane which happens to reside near a phase transition boundary may undergo an abrupt change in the phase structure with a small change in lipid composition or external conditions (e.g. temperature) and thereby exhibit a potentially large change in solute permeability. Indeed, several studies have demonstrated sharp maxima in solute permeability in the two-phase coexistence regions which exist at the main phase transition between the gel and liquid crystalline states in single component lipid bilayers [28–35] and over a broader temperature range in DMPC/DPPC bilayers [36,37].

The main objective of this study is to understand how changes in bilayer phase structure in dipalmitoylphosphatidylcholine (DPPC)/CHOL, dihexadecylphosphatidylcholine (DHPC)/CHOL, or DPPC/dimyristoylphosphatidylcholine (DMPC) bilayers affect the permeability of two small model permeants (acetic acid and trimethylacetic acid). Changes in bilayer phase structure were induced by changes in temperature (20–53°C) and lipid composition ($X_{CHOL} = 0.0–0.55$ and $X_{DMPC} = 0.0–1.0$). In particular, these studies address the variation of solute permeability with chemical composition and temperature in three types of thermodynamic phases [the cholesterol-poor disordered liquid-crystalline phase (L_α), the cholesterol-rich ordered liquid-crystalline phase (L_o), and the gel phases (P'_β and $L_{\beta i}$)] and in the various two-phase coexistence regions between these three types of phase domains. CHOL and DMPC were selected as one of the bilayer components in the binary lipid bilayers as they mix non-ideally with DPPC and/or DHPC lipids due to mismatches in lipid flexibility and chain length, respectively. Moreover, biological membranes possess phospholipids of various chain lengths and may contain cholesterol compositions as high as 50 wt% of the total lipid (e.g., human erythrocytes). As in our previous studies [38,39], the permeability coefficients for acetic acid and trimethylacetic acid were measured in large unilamellar vesicles (LUVs) using a combined method of NMR line-broadening and dynamic light scattering.

2. Experimental

2.1. Materials

DPPC and DMPC were purchased from Avanti Polar Lipids (Pelham, AL). DHPC (99%) and CHOL (99 + %) were purchased from Sigma (St. Louis, MO). These lipids were stored in a −20°C freezer

upon arrival. Acetic acid (99.8%) and trimethylacetic acid (99%) were purchased from Aldrich (Milwaukee, WI). All other reagents were obtained commercially and were of analytical reagent grade.

2.2. LUV liposome preparation

LUVs were prepared by a modified combined technique due to Bangham et al. [40] and Olson et al. [41], a detailed description of which has been published elsewhere [38]. Briefly, phospholipid (5–10 mg) and cholesterol (0–5 mg) were accurately weighed and dissolved in chloroform. The solution was evaporated under nitrogen gas to a dry thin film on the bottom of a round-bottom test tube and left under vacuum for 2 h at ≈ 50°C. A 1 ml aqueous solution containing 5–50 mM acetic acid or 5–20 mM trimethylacetic acid at a given pD was then added and the lipids were hydrated by repeated vortexing and shaking at a temperature above the main transition temperature for DPPC or DHPC. The multilamellar vesicles (MLVs) formed were forced through a polycarbonate filter (0.1 or 0.2 μm, Nuclepore®) 17 times to form LUVs before the NMR transport experiments.

2.3. Determination of permeability coefficients across lipid bilayers

The lifetimes for acetic acid and trimethylacetic acid in the entrapped aqueous volume of LUVs were determined as a function of lipid concentration and temperature by the ^{1}H-NMR line-broadening method originally developed by Alger and Prestegard [42] and recently validated in this laboratory [38]. Both acetic acid and trimethylacetic acid have single proton peaks at ≈ 1.9 ppm and 1.1 ppm, respectively. The addition of a small amount of an impermeable shift reagent, $Pr(NO_3)_3$, to a final concentration of 1–5 mM in LUVs before the spectral acquisition causes a down-field shift of the proton resonance frequency for an extravesicular permeant (ω_o) while the proton resonance frequency for an entrapped permeant (ω_i) remains unchanged. The line-widths of both peaks broaden as a result of transport across the LUVs. The binding capacity of the chemical shift reagent (Pr^{+3}) and its effects on solute permeability (P_m) have been studied previously [38]. These studies established that the P_m for acetic acid in the two-phase region in DMPC/CHOL ($X_{CHOL} = 0.2$) is independent of $[Pr^{+3}]$ for $[Pr^{3+}] < 40$ mM. The actual concentration of free Pr^{+3} available for binding to the outer vesicle surface is lower than the total Pr^{+3} concentration used as acetic acid in solution also forms complexes with Pr^{+3}. For example, at $[Pr^{+3}] = 5$ mM and a total acetic acid concentration of 0.05 M (pD = 6.32), only one quarter of the total Pr^{+3} would exist in the uncomplexed form.

The experiments were performed on a Bruker-200 NMR spectrometer (Bruker Instruments, Billerica, MA) operated in the Fourier transform mode at 200 MHz. Samples were equilibrated for 20 min at a given temperature controlled by a standard variable temperature accessory (BVT1000, Bruker). Each spectrum was the average of 32–1000 acquisitions separated by a pulse delay of 2–4 s. The spectra were Fourier transformed and phased with an ASPECT 3000 computer.

In the slow exchange limit, $|\omega_i - \omega_o|T_{2,i} >> 1$, the line-width of the unshifted proton peak is related to the lifetime of the entrapped permeants inside the vesicle, τ_i, by the following line-width expression [43]

$$\pi\Delta\nu = 1/\tau_i + 1/T_{2,i} \quad (1)$$

where $\Delta\nu$ is the full line-width at one-half the maximum peak height and $T_{2,i}$ is the spin-spin relaxation time which includes heterogeneous line broadening in the absence of exchange. The line-width in the absence of exchange ($1/T_{2,i} = 2.5$–4.0 Hz) was obtained at a low temperature and/or high pD where the permeation rate is negligible.

Since the permeability of ionized permeants is negligible in the pD range of interest [38,44,45], the permeability coefficient for the neutral species, P_m, can be expressed as

$$P_m = \frac{V}{\tau_i A_t}\frac{([D^+] + K_a)}{[D^+]} \quad (2)$$

where V is the entrapped volume, A_t is the vesicle surface area, and K_a is the dissociation constant in D_2O. K_a is 7.55×10^{-6} for acetic acid [46] and was determined for trimethylacetic acid in the present

study by pD titration to be $(3.16 \pm 0.05) \times 10^{-6}$. The V/A_t ratio was determined from the hydrodynamic diameter (d) as obtained from dynamic light scattering (DLS) measurements according to the formula

$$V/A_t = (d - \Delta r)/6 \quad (3)$$

where Δr is the bilayer thickness. The apparatus for DLS studies consisted of a photon correlation spectrometer (Model BI-90, Brookhaven Instruments, Holtsville, NY) and a He-Ne laser light source at 632.8 nm wavelength. One drop of LUV suspension was placed in a 13×75 mm clean glass test tube and diluted to 2 ml with the same filtered solution used to prepare the LUVs but with 1–5 mM Pr^{3+} added. The sample was placed in a temperature-controlled cuvette holder with a toluene index-matching bath. Autocorrelation functions were determined over 100 s with a 10–80 μs duration at 90°C and analyzed by the method of cumulants.

3. Results and discussion

Fig. 1 displays representative NMR signals for the methyl protons of entrapped acetic acid (panel A) in DHPC/CHOL vesicles ($X_{CHOL} = 0.2$) at pD = 5.69 and entrapped trimethylacetic acid (panel B) in DPPC/CHOL vesicles ($X_{CHOL} = 0.2$) at pD = 7.10 at various temperatures. Line-widths at one-half the maximum peak height, from which permeability coefficients were determined according to Eqs. (1) and (2), are also shown. The strong dependencies of the proton line widths on temperature for both permeants correspond to rather dramatic increases in permeability coefficients of an order-of-magnitude or more over a narrow temperature range of ≤ 10°C, suggesting that permeability data may be useful in probing changes in bilayer phase structure.

3.1. DHPC / CHOL bilayers

Although in most phospholipids of biological interest the hydrocarbon chains are attached to the glycerol moiety through an ester linkage, ether-linked phospholipids occur in significant proportions in a variety of mammalian tissues [47]. The influence of the type of linkage on the non-ideality of phospholipid mixing with cholesterol has not been fully characterized. Permeability coefficients for acetic acid across ether-linked DHPC/CHOL bilayers of different $X_{CHOL}(= 0.0–0.5)$ were determined at six temperatures: 33°C, 36°C, 40°C, 41°C, 47°C, and 53°C (four below and two above the DHPC main transition temperature of 43–45°C [48,49]). Semi-logarithmic plots of P_m versus X_{CHOL} are presented in Fig. 2. The solid lines in Fig. 2 represent linear fits of the data in the regions of low and high CHOL composition prior to or after apparent break points. These apparent break points are connected by dashed lines. (Though regions of linearity are evident in these plots within the single phase regions, there is no theoretical basis for such a relationship at present.)

At 33°C, slightly below the pretransition temperature for DHPC representing its conversion from a hexagonally packed interdigitated phase ($L_{\beta i}$) to the conventional non-interdigitated gel phase bilayer (P'_β) [48–50], a small amount of CHOL ($X_{CHOL} \leq 0.05$) reduces P_m by roughly two-fold. Addition of more CHOL starts to increase P_m before reaching a turning point at $X_{CHOL} = 0.35$, above which P_m again declines with further CHOL addition. At 33°C, the addition of a small amount of CHOL ($X_{CHOL} \leq 0.05$) appears to induce a transition from the interdigitated gel phase ($L_{\beta i}$) to the conventional non-interdigitated gel phase (P'_β) [48,49]. Along with this phase transition the bilayer thickness increases by roughly two-fold, which may be one factor accounting for the observed permeability decrease with increasing CHOL at $X_{CHOL} < 0.05$.

Above the pretransition temperature but below T_m and at $X_{CHOL} \leq 0.05$, the DHPC/CHOL bilayers are in the non-interdigitated gel phase and the permeability coefficient of acetic acid increases only modestly with CHOL concentration. Abrupt changes of P_m (i.e., break points) are observed at $X_{CHOL} = 0.05$ and 0.35 at both 36°C and 40°C, between which the permeability coefficient increases more dramatically with CHOL concentration. Above $X_{CHOL} = 0.30–0.35$, the permeability coefficient starts to decline, reversing the trend at the lower CHOL concentration. The break points at lower and higher CHOL concentrations presumably mark the phase boundaries between two different phases, while the regions indicated by the dashed lines correspond to the two-phase

coexistence region. The dashed lines connecting the P_m values at the two break points are predicted from a two-phase model (cf., Eqs. (4) and (5)) assuming simple averaging of the permeability coefficients across each phase. Below T_m, the slopes of the dashed lines become less positive with increasing temperature, approaching zero near the main transition.

Above the main transition temperature for DHPC (43–45°C), except in a narrow range between X_{CHOL} of 0.05 and 0.10 where P_m abruptly increases, the permeability coefficient of acetic acid decreases

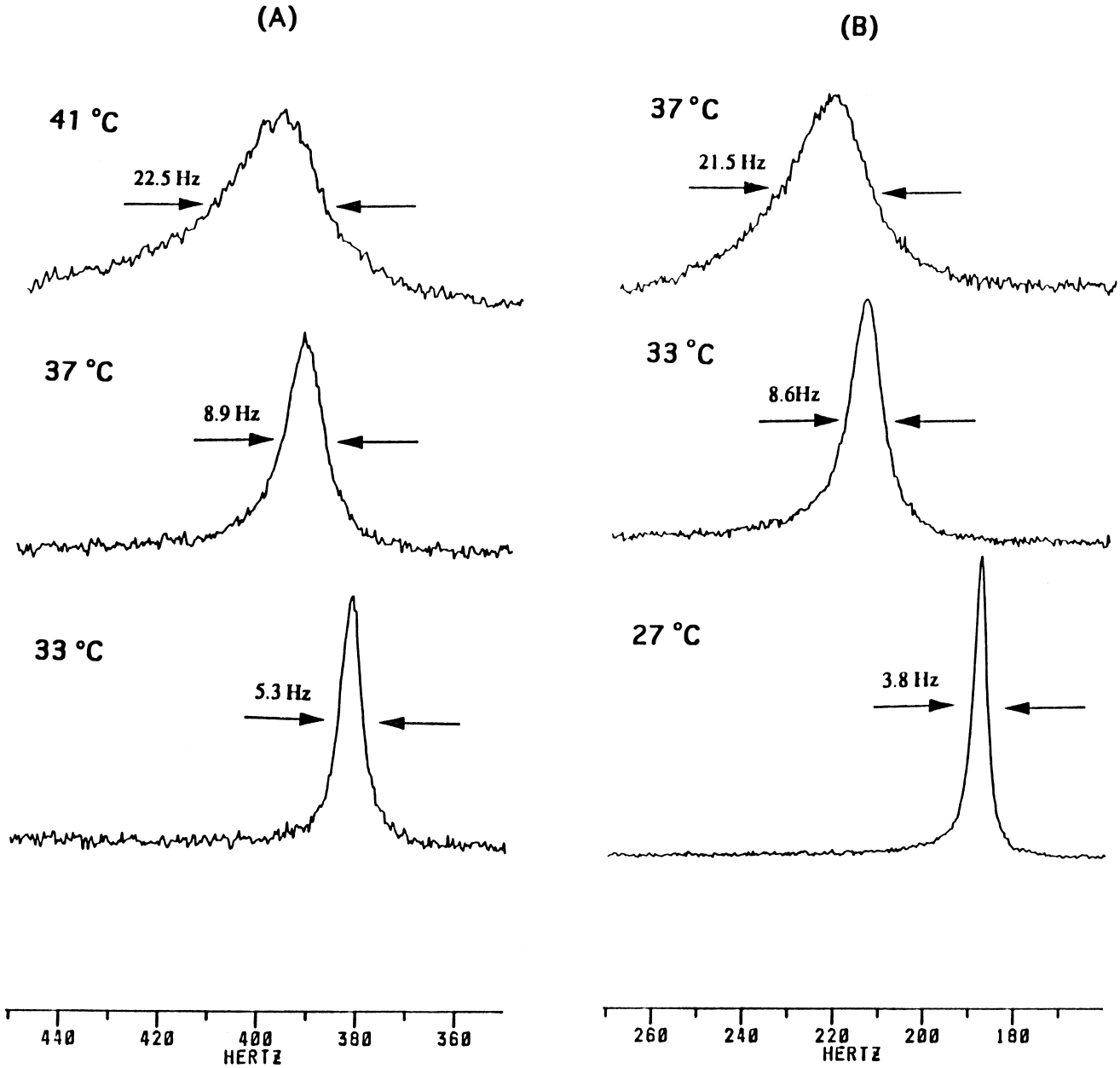

Fig. 1. Panel A: NMR signals for the methyl protons of entrapped acetic acid at pD = 5.69 across DHPC/CHOL bilayers (X_{CHOL} = 0.2) at 33°C, 37°C and 41°C. Panel B: NMR signals for the methyl protons of entrapped trimethylacetic acid at pD = 7.10 across DPPC/CHOL bilayers (X_{CHOL} = 0.2) at 27°C, 33°C, and 37°C. Line widths at one-half maximum peak height are shown.

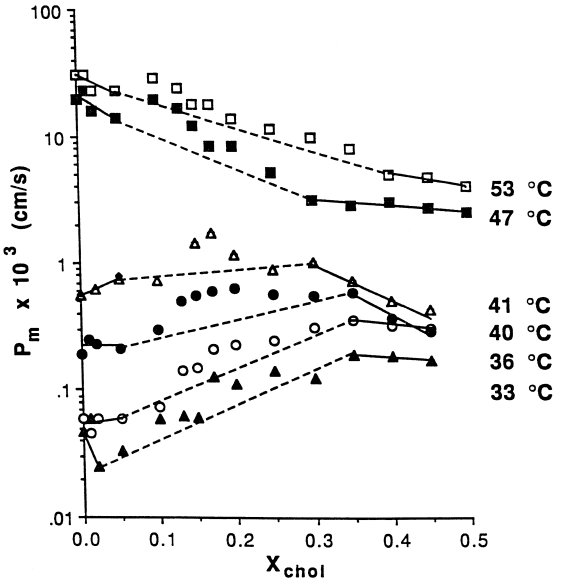

Fig. 2. The permeability coefficient (P_m) for acetic acid across DHPC/CHOL bilayers versus the mole fraction concentration of cholesterol, X_{CHOL}, at six constant temperatures (33°C, 36°C, 40°C, 41°C, 47°C and 53°C). The dashed lines are drawn from the two break points to demonstrate the deviations of the experimental data from the two-phase model.

monotonically with CHOL concentration. P_m decreases with X_{CHOL} more steeply at low CHOL concentration than at high CHOL concentration. This parallels the ordering effects of CHOL on phospholipids, being more pronounced at low CHOL concentration and levelling off at high CHOL concentration [51]. The abrupt increase of P_m in the narrow range of $X_{chol} = 0.05–0.10$ corresponds to the beginning of a two-phase coexistence region, due to the appearance of a cholesterol-rich ordered liquid-crystalline phase when more than 5 mol% cholesterol is added to DHPC bilayers [49].

Vist and Davis [21] and others earlier [52,53] have shown that CHOL disrupts largely all-trans chain conformations and increases lipid lateral diffusion and axial rotation in the gel phase, while in liquid-crystalline phases, CHOL increases lipid chain orientational order due to stiffening of the lipid chains promoted by the rigid surface of cholesterol. At low CHOL concentration, the slopes of the semilogarithmic plots of P_m vs. X_{CHOL} in Fig. 2 are consistent with these observations, as small positive slopes are evident in the non-interdigitated gel phase (P'_β) but large negative values are found in the disordered liquid-crystalline phase (L_α). We have previously demonstrated that the bilayer chain-ordering effects of CHOL, temperature, and acyl chain length in both gel and liquid-crystalline single phase bilayers influence P_m in a manner which can be quantitatively accounted for by an exponential dependence of P_m on free surface area [54].

Binary bilayer membranes composed of phospholipid and CHOL have been shown to behave non-ideally, exhibiting a complex phase structure. At present, the complete phase diagram for DHPC/CHOL bilayers is not available, but studies by Laggner et al. [49] have shown that DHPC/CHOL and DPPC/CHOL bilayers have similar phase structures. Fig. 3 presents the temperature-composition phase diagram for DHPC/CHOL bilayers constructed from the break points estimated from the permeability data in Fig. 2. These break points presumably delineate the boundaries between various phase domains. The phase diagram shows a two-phase (P'_β–L_o) coexistence region below T_m. The solidus (CHOL-poor) boundary is roughly vertical within ten degrees of T_m, while the liquidus (CHOL-rich) boundary tilts

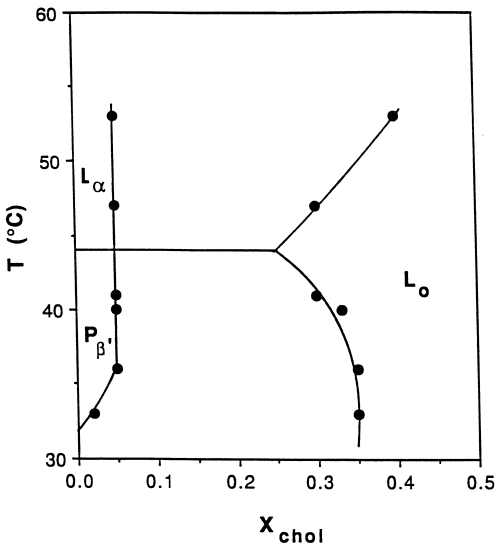

Fig. 3. The temperature-composition phase diagram for DHPC/CHOL bilayers from permeability data. The data points are obtained from the $P_m - X_{CHOL}$ profiles in Fig. 2. The solid curves are drawn through the data points assuming a T_m for DHPC of 44°C.

towards higher CHOL concentrations above T_m and within a few degrees below T_m, but becomes vertical when temperature is further lowered.

One of the most striking features of the plots in Fig. 2 are the oftentimes large positive deviations of the permeability coefficients from the dashed lines connecting the single phase values. The largest deviations generally occur closer to the CHOL-poor solidus boundary. Since the phase lever rule predicts a linear dependence of P_m on X_{CHOL} in the two-phase coexistence region (vide infra), the positive deviations observed suggest that alternative transport mechanisms must be considered in bilayers containing two or more coexisting phase domains (see Section 2.3).

3.2. DPPC / CHOL bilayers

The permeability coefficients for acetic acid across DPPC/CHOL bilayers of different X_{CHOL} (= 0.0–0.5) were determined at five temperatures: 30°C, 33°C, 37°C, 44°C, and 50°C (three below and two above the DPPC main transition temperature of T_m = 41°C [17,21,25,55,56]). These temperatures were chosen so that the experiments were performed at reduced temperatures similar to those employed in DHPC/CHOL bilayers. The results are presented as semi-logarithmic plots of P_m vs. X_{CHOL} in Fig. 4. At 33°C and 37°C at $X_{CHOL} \leq 0.05$, the permeability coefficients increase only slightly with CHOL concentration. Above $X_{CHOL} = 0.05$, abrupt increases in the slopes are evident until at $X_{CHOL} \approx 0.34$ at 30°C, 0.25 at 33°C, and 0.20 at 37°C when P_m values start to decline, reversing the trend at lower CHOL concentrations. At 30°C (i.e., below the pretransition between the gel phases L'_β and P'_β), only one break point at $X_{CHOL} = 0.34$ is observed. Evidently, below the pretransition, which represents a change in lipid packing from an orthorhombic to a hexagonal subcell, the DPPC gel phase domain is immiscible with even a very small amount of cholesterol, such that separate formation of the cholesterol-rich liquid-ordered phase occurs at very low X_{CHOL}.

As in DHPC/CHOL bilayers, above the main transition temperature for DPPC, except in a narrow range between X_{CHOL} of 0.05 and 0.10 where an abrupt change in the slope occurs, P_m decreases with CHOL concentration, in contrast to what is observed below T_m. P_m decreases with X_{CHOL} more steeply at low CHOL concentration than at high CHOL concentration, again paralleling the ordering effects of CHOL on phospholipids, being more pronounced at low CHOL concentration and levelling off at high CHOL concentration [51]. The abrupt increases in P_m in the narrow range of $X_{chol} = 0.05–0.10$ correspond to the beginning of a two-phase coexistence region, due to the appearance of a cholesterol-rich ordered liquid-crystalline phase when more than 5 mol% cholesterol is added to DPPC bilayers [17,18,21,55,57]. As in DHPC/CHOL bilayers, the slope in the log P_m vs. X_{CHOL} plot is a small positive value in the gel phase (P'_β) but a large negative value in the disordered liquid-crystalline phase (L_α). In the L_o phase, which may be an appropriate model of high cholesterol-containing natural plasma membranes, the slope is invariably slightly negative and nearly independent of temperature in the region of 33–50°C.

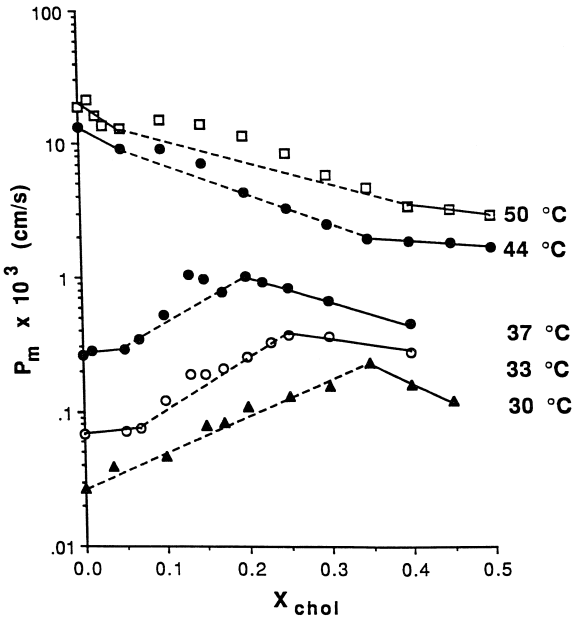

Fig. 4. The permeability coefficient (P_m) for acetic acid across DPPC/CHOL bilayers versus the mole fraction concentration of cholesterol, X_{CHOL}, at five constant temperatures (30°C, 33°C, 37°C, 44°C and 50°C). The dashed lines are drawn from the break points to demonstrate the deviations of the experimental data from the two-phase model.

Phase diagrams for the DPPC/CHOL bilayer system have been generated from various spectroscopic studies and theoretical simulations (see, e.g., [17,18,21,55,57]. Although these diagrams are gener-

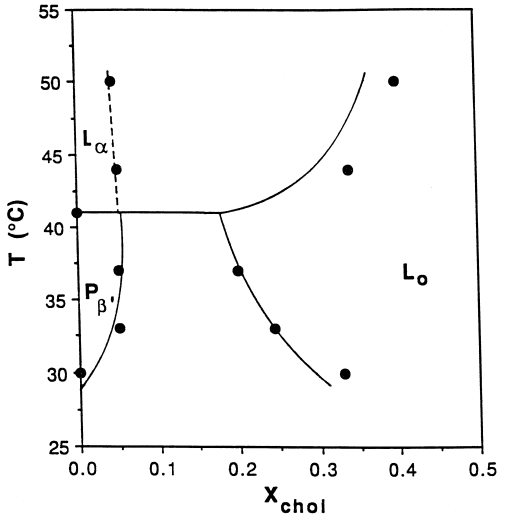

Fig. 5. The temperature-composition phase diagram for DPPC/CHOL bilayers. The solid boundary curves are drawn from the ^{2}H- and ^{13}C-NMR data by Huang et al. [18]. The dashed line drawn through the permeability data was not included in Huang's phase diagram. The data points are obtained from the $P_m - X_{CHOL}$ profiles in Fig. 4.

ally similar, some discrepancies do exist. The solid curves in Fig. 5 display the phase diagram for DPPC/CHOL bilayers obtained by Huang et al. [18] using a combined ^{13}C- and ^{2}H-NMR method. For comparison, the break points apparent from the permeability data in Fig. 4, which presumably delineate the boundaries between various phase domains, are also plotted in Fig. 5. These data are in general agreement with the phase boundaries below T_m and the L_α–L_o boundary for CHOL-rich bilayers elucidated by Huang et al. [18]. Such close agreement supports the notion that changes in both trans-bilayer permeability and various spectroscopic measurements are capable of probing the same fundamental changes in bilayer phase structure. One of the significant differences in the phase diagrams in the literature is the delineation of the liquidus boundary between the phases P'_β and L_o below T_m. Both the present results and those of Huang et al. define the two-phase coexistence region with the liquidus boundary tilting toward a higher X_{CHOL} value when temperature decreases. This structural feature agrees with a theoretical study by Ipsen (1989) using a mean-field approximation. However, it is in contrast with earlier studies of DPPC/CHOL bilayers [21,58,59] in which a roughly vertical liquidus line at $X_{CHOL} \approx 0.2$ was suggested and differs also from the behavior of DHPC/CHOL bilayers reported above.

Controversy also exists regarding the occurrence of a two-phase coexistence region between the liquid-crystalline phases, L_α and L_o, which converges at a critical temperature. Most of the earlier experimental and theoretical studies suggested the existence of this two-phase region in DPPC/CHOL bilayers [17,21,55,57] but more recently, Huang and coworkers found experimental evidence disputing some of the earlier DSC and ^{2}H-NMR results from which the boundary between the L_α phase and the two-phase coexistence region above T_m was constructed [18]. In particular, Huang and coworkers found higher temperatures for the end of melting of a broad DSC peak than those reported and failed to observe the sharpening of the ^{2}H-NMR resonances (Vist and Davis, 1990). In the phase diagram drawn by Huang et al. (1993), the liquidus boundary defining a two-phase coexistence region above T_m is notably absent. Break points near $X_{CHOL} = 0.05$ are clearly apparent, however, in the present study (cf., Fig. 4), even at temperatures above T_m, and likely reflect the boundary between the L_α liquid-crystalline phase and the L_α–L_o two-phase coexistence region.

To explore whether or not the choice of permeant is critical in generating phase diagrams from permeability data, the permeability coefficient for a significantly larger permeant, trimethylacetic acid (TMAA) was also determined across DPPC/CHOL bilayers as a function of CHOL concentration at three constant temperatures (30°C, 33°C, and 37°C). Permeability values of TMAA could not be determined above T_m due to its higher lipophilicity, and consequently higher permeability coefficient, in comparison to acetic acid. The results are presented in Fig. 6. In general, the P_m–X_{CHOL} profiles for TMAA resemble those for acetic acid (Fig. 4) indicating that the strong correlation between solute permeability and bilayer phase properties is not unique to acetic acid. However, some subtle differences exist. For example, an apparent phase boundary at 30°C between $X_{CHOL} = 0.05$–0.l0 suggested by the TMAA data was ignored due to its absence in the data for acetic acid.

Clearly evident in both Fig. 4 and Fig. 6 are the significant positive deviations of the observed perme-

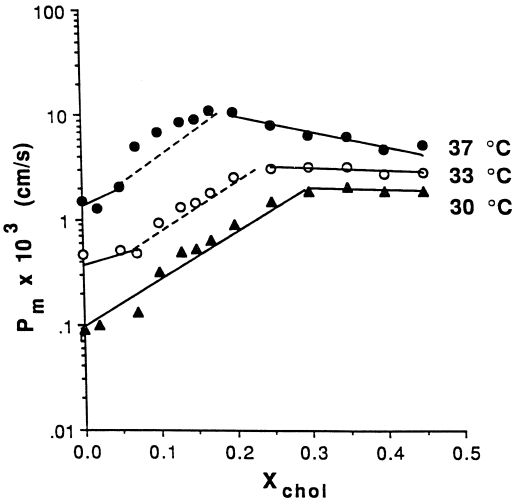

Fig. 6. The permeability coefficient (P_m) for trimethylacetic acid across DPPC/CHOL bilayers versus the mole fraction concentration of CHOL, X_{CHOL}, at three constant temperatures (30°C, 33°C and 37°C) below T_m (DPPC). The dashed lines are drawn from the two break points to demonstrate the deviation of the experimental data from the two-phase model.

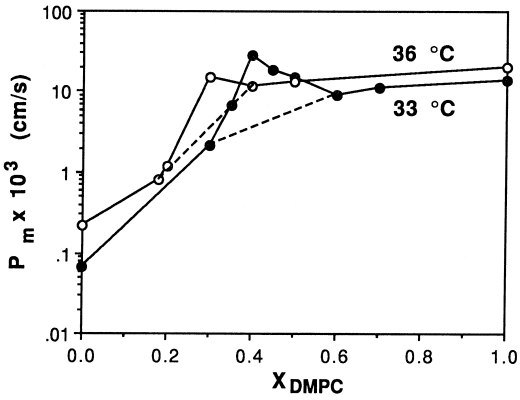

Fig. 7. The permeability coefficient (P_m) for acetic acid across DPPC/DMPC bilayers versus the mole fraction concentration of DMPC, X_{DMPC}, at two constant temperatures 33°C (●) and 36°C (○). The dashed lines are drawn from the two break points to demonstrate the deviations of the experimental data from the two-phase model.

ability coefficients at 33°C, 37°C, 44°C and 50°C from the dashed lines connecting the P_m values at the two single phase boundaries. The magnitude of this deviation decreases with temperature and is virtually undetectable in the gel-L_o coexistence region at 30°C. In most instances, as seen previously in DHPC/CHOL bilayers, the maxima in these deviations appear to occur closer to the solidus boundaries (i.e., at low CHOL concentration).

3.3. DPPC / DMPC bilayers

Permeability coefficients for acetic acid were determined in DPPC/DMPC bilayers as a function of X_{DMPC} at two fixed temperatures, 33°C and 36°C, and as a function of temperature at several values of X_{DMPC}. The dependence of acetic acid's permeability coefficient on X_{DMPC} at 33°C and 36°C is illustrated in Fig. 7. Previously published phase diagrams for DPPC/DMPC bilayers constructed from ESR and DSC results [56,60,61] indicate that at 36°C liquid-crystalline and gel phases coexist between $X_{DMPC} \approx$ 0.2–0.4 while at 33°C this two-phase coexistence region lies between $X_{DMPC} \approx 0.3$–0.6. As shown by Fig. 7, permeability maxima are observed within the two-phase coexistence regions at $X_{DMPC} = 0.30$ and 36°C and $X_{DMPC} = 0.40$ and 33°C. In the single-phase regions, P_m increases with DMPC concentration but the effects of DMPC concentration on P_m are markedly different in gel and liquid-crystalline phases. In the liquid-crystalline phases (i.e., at $X_{DMPC} > 0.5$–0.6) P_m varies only by a factor of ≈ 2, whereas in the gel phases (i.e., at $X_{DMPC} < 0.2$–0.3) P_m varies by more than one order of magnitude.

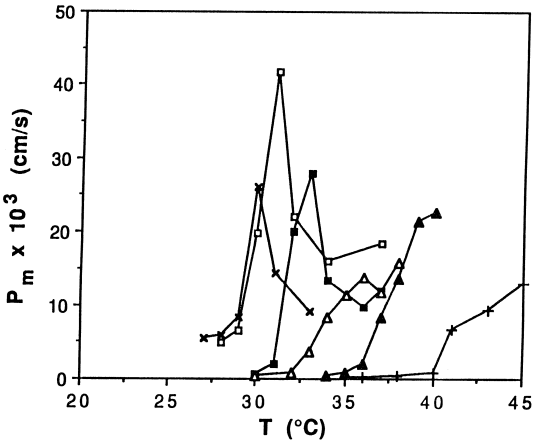

Fig. 8. The permeability coefficient (P_m) for acetic acid across DPPC/DMPC bilayers versus temperature at six constant DMPC concentrations: $X_{DMPC} = 0.0$ (+), 0.2 (▲), 0.3 (△), 0.4 (■), 0.5 (□) and 0.6 (×).

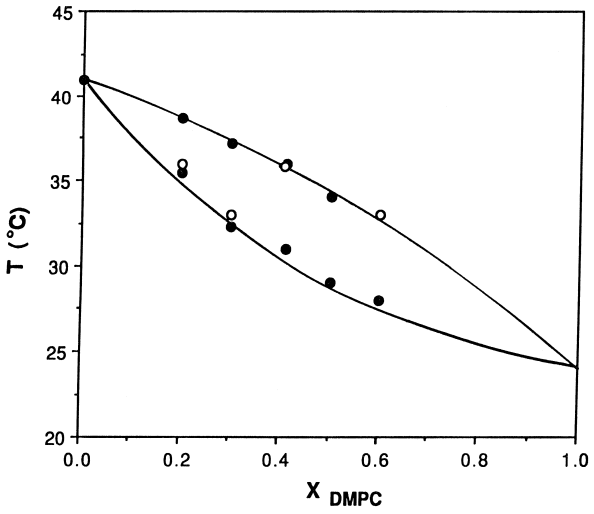

Fig. 9. The temperature-composition phase diagram for DPPC/DMPC bilayers: the open circles are the break points in Fig. 7 and the closed circles are the break points in Fig. 8. The solid boundary curves are drawn from statistical mechanical calculations by Jacobs et al. [61] based on ESR and DSC data [56,60].

Fig. 8 displays the permeability coefficients for acetic acid obtained at several constant X_{DMPC} values as a function of temperature. At low temperatures and in gel-state bilayers, permeability coefficients are very small and increase only modestly with temperature. Sudden changes in P_m (i.e., break points) observed at 36°C and 39°C at $X_{DMPC} = 0.2$, 32°C and 37°C at $X_{DMPC} = 0.3$, 31°C and 36°C at $X_{DMPC} = 0.4$, 29°C and 34°C at $X_{DMPC} = 0.5$, and 28°C and 33°C at $X_{DMPC} = 0.6$ presumably delineate the boundaries between different phase domains. These break points are plotted in Fig. 9 along with the literature phase diagram for DPPC/DMPC bilayers constructed previously based on ESR and DSC results [56,60,61]. Close agreement with the thermodynamic and spectroscopic results is noted, which, once again, supports the notion that trans-bilayer permeability measurements are a sensitive means of detecting phase boundaries in lipid bilayers.

As seen in Fig. 8, permeability maxima are observed a few degrees above the low-temperature break points corresponding to the two-phase coexistence regions. The largest permeability maximum occurs at $X_{DMPC} = 0.5$ with the magnitude of the maxima decreasing with a decrease (or increase) in X_{DMPC}, becoming invisible at $X_{DMPC} \leq 0.2$. Similar maxima have been reported for the permeabilities of glucose and a small zwitterionic molecule, methyl-phosphoethanolamine, in DPPC/DMPC bilayers within the region where DPPC-enriched gel phase domains coexist with DMPC-enriched liquid-crystalline domains [37].

3.4. Permeability in the two-phase coexistence region

^{13}C-NMR spin relaxation [62] and molecular dynamics simulation [63] studies have shown that the diffusion coefficients for small molecules (e.g., di-*tert*-butyl nitroxide and benzene) within phospholipid bilayers are on the order of $(0.5–5) \times 10^{-6}$ cm^2/s, 1–4 orders of magnitude faster than the lateral diffusion rates of lipids responsible for the exchange between different phase domains. Thus, within a two-phase coexistence region of a binary lipid bilayer, a permeating solute may traverse the bilayer by two distinct transport routes through phase 1 and phase 2 domains with the respective permeability coefficients of P_1 and P_2. Such a model would lead to the following expression for the overall permeability coefficient P_m

$$P_m = (1 - f_2) P_1 + f_2 P_2 \quad (4)$$

where f_2 is the fraction of the phase 2 domain, obtainable from the following lever rule,

$$f_2 = \frac{X - X_1}{X_2 - X_1} \quad (5)$$

In Eq. (5), X_1 and X_2 are the lipid mole fraction concentrations at the phase 1 and phase 2 boundaries, respectively. According to this two-phase model, the overall permeability P_m would be expected to change linearly with DMPC (or CHOL) concentration in DPPC/DMPC bilayers (or DPPC/CHOL and DHPC/CHOL bilayers).

Referring to Figs. 2, 4, 6 and 7, it is clear that the permeability coefficients for acetic acid and TMAA exhibit significant positive deviations from the dashed line predictions of the lever rule in the two-phase regions for DHPC/CHOL, DPPC/CHOL, and DPPC/DMPC bilayers. In DHPC/CHOL and DPPC/CHOL bilayers, the maximum deviations appear to occur near the CHOL-poor boundaries above the main transition of the corresponding phospholipid

but close to the middle of the two-phase region at temperatures below the main transition. In DPPC/DMPC bilayers, the permeability maxima occur near the middle of the two-phase region. The persistent observation of these positive deviations in all three bilayers studied, combined with demonstrations of permeability maxima within the two-phase coexistence regions in previous studies of both single-component and two-component bilayers [28–37] suggests that this is a universal phenomenon that cannot be accounted for by the above two-phase domain transport model. Instead, this behavior within two-phase coexistence regions is believed to be associated with unusual density fluctuations in the transition region where two or more phases coexist. While some investigators have argued that the permeability maximum in a phase transition can be attributed to the high lateral compressibility of bilayers in this region [32,64–66], others suggest that enhanced permeabilities are attributable more specifically to a distinct property of the interfacial region [33–35,37,67].

4. Concluding remarks

The permeability properties of lipid bilayers depend on lipid composition in a complex but somewhat predictable manner. Additions of a second lipid component to a phospholipid bilayer may have profound effects on solute permeability, depending on the mismatches between these two types of lipids. Short and flexible acyl-chain lipids (e.g, DMPC addition to DPPC bilayers) increase solute permeability coefficients in single phase gel and liquid-crystalline bilayers with their effects being the greatest in the gel phase. This is analogous to the enhancement effects observed for fatty acids [68,69] on drug permeability across stratum corneum, and suggests a common mechanism for the effects of intercalated short-chain molecules on solute permeation. Bulky and rigid cholesterol molecules decrease P_m in single liquid-crystalline phases and increase P_m slightly in gel phases. Generally, P_m decreases with X_{CHOL} more substantially when the bilayer is in a more disordered state (e.g., at low cholesterol concentration and high temperature). Positive deviations from a simple two-phase domain transport model are observed in the two-phase coexistence regions. These deviations may be rationalized either by higher lateral compressibility in the two-phase coexistence region or by an additional interfacial transport pathway.

Abrupt changes in permeabilities of acetic acid and trimethylacetic acid observed at the phase boundaries in lipid bilayer membranes indicate that the measurement of trans-bilayer permeation rates may be useful in mapping phase diagrams for lipid bilayers. Permeability methods may offer some advantages over existing methods for the determination of bilayer phase structure. For example, as pointed out by Huang et al. [18], considerable difficulties exist in establishing a correct interpretation of results from differential scanning calorimetry (DSC), one of the most widely used methods for studying bilayer phase structure, because of the extremely broad transitions in the presence of cholesterol and non-reproducibility of the baselines. Fluorescence recovery after photobleaching [70] and ESR [57] experiments require the use of probe molecules whose size and concentrations in the bilayer interior are generally much greater than those for the permeants used in the present study. The perturbation of local bilayer structure by these probe molecules is not entirely understood. ^{2}H- and ^{13}C-NMR spectra are useful in characterizing liquid-crystalline and gel phases, respectively, but require the labelling of lipid molecules, and their quantitative analyses (spectral simulations) are not as straightforward as the permeability method, and sometimes difficult due to the complex conformational motions of lipids [18,21].

Acknowledgements

This work was supported by grants from National Institute of Health (RO1 GM51347-01A2) and the University of Utah Research Committee.

References

[1] R. Welti, M. Glaser, Chem. Phys. Lipids 73 (1994) 121–137.
[2] L.D. Bergelson, Topical Issue Mol. Membr. Biol. 12 (1995) 1–91.
[3] P.K.J. Kinnunen, Chem. Phys. Lipids 57 (1991) 375–399.

[4] D.B. Fenske, J.L. Thewalt, M. Bloom, N. Kitson, Biophys. J. 67 (1994) 1562–1573.
[5] E. ten Grotenhuis, R.A. Demel, M. Ponec, D.R. Boer, J.C. van Miltenburg, J.A. Bouwstra, Biophys. J. 71 (1996) 1389–1399.
[6] S.H. White, D. Mirejovsky, G.I. King, Biochemistry 27 (1988) 3725–3732.
[7] C.R. Mateo, A.U. Acuna, J.-C. Brochon, Biophys. J. 68 (1995) 978–987.
[8] S.C. Chen, J.M. Sturtevant, Biochemistry 20 (1981) 713–718.
[9] J.Y.A. Lehtonen, M.M. Holopainen, P.K.J. Kinnunen, Biophys. J. 70 (1996) 1753–1760.
[10] D.L. Melchior, Science 234 (1986) 1577–1580.
[11] J. Huang, J.E. Swanson, A.R. Diddle, A.K. Hinderliter, G.W. Feigenson, Biophys. J. 64 (1993) 613–625.
[12] A.K. Hinderliter, J. Huang, G.W. Feigenson, Biophys. J. 67 (1994) 1906–1911.
[13] J.Y.A. Lehtonen, P.K.J. Kinnunen, Biophys. J. 72 (1997) 1247–1257.
[14] P. Mustonen, J.A. Virtanen, P.J. Somerharju, P.K.J. Kinnunen, Biochemistry 26 (1987) 2991–2997.
[15] E.S. Rowe, Biochemistry 26 (1987) 46–51.
[16] P.F.F. Almeida, W.L.C. Vaz, T.E. Thompson, Biochemistry 31 (1992) 7198–7210.
[17] J.H. Ipsen, G. Karlstrom, O.G. Mouritsen, H. Wennerstrom, M.J. Zuckermann, Biochim. Biophys. Acta 905 (1987) 162–172.
[18] T.-H. Huang, C.W.B. Lee, S.K. Das Gupta, A. Blume, R.G. Griffin, Biochemistry 32 (1993) 13277–13287.
[19] T.P.W. McMullen, R.N.A.H. Lewis, R.N. McElhaney, Biochemistry 32 (1993) 516–522.
[20] T.P.W. McMullen, R.N.A.H. Lewis, R.N. McElhaney, Biophys. J. 66 (1994) 741–752.
[21] M.R. Vist, J.H. Davis, Biochemistry 29 (1990) 451–464.
[22] D. Tang, B.W. Van Der Meer, S.-Y.S. Chen, Biophys. J. 68 (1995) 1944–1951.
[23] T. Parasassi, A.M. Giusti, M. Raimondi, E. Gratton, Biophys. J. 68 (1995) 1895–1902.
[24] B. Snyder, E. Friere, Proc. Natl. Acad. Sci. U.S.A. 77 (1980) 4055–4059.
[25] D.L. Melchior, F.J. Scavitto, J.M. Steim, Biochemistry 19 (1980) 4828–4834.
[26] J.A. Virtanen, M. Ruonala, M. Vauhkonen, P. Somerharju, Biochemistry 34 (1995) 11568–11581.
[27] M.B. Sankaram, D. Marsh, T.E. Thompson, Biophys. J. 63 (1992) 340–349.
[28] M.C. Blok, E.C.M. van der Neut-Kok, L.M.M. van Deenen, J. De Gier, Biochim. Biophys. Acta 406 (1975) 187–196.
[29] M.C. Blok, L.M.M. van Deenen, J. de Gier, Biochim. Biophys. Acta 433 (1976) 1–12.
[30] J. Bramhall, J. Hofmann, R. DeGuzman, S. Montestruque, R. Schell, Biochemistry 26 (1987) 6330–6340.
[31] E.M. El-Mashak, T.Y. Tsong, Biochemistry 24 (1985) 2884–2888.
[32] A. Georgallas, J.D. McArthur, X.P. Ma, C.V. Nguyen, G.R. Palmer, M.A. Singer, M.Y. Tse, J. Chem. Phys. 86 (1987) 7218–7226.
[33] D. Marsh, A. Wats, P.F. Knowles, Biochim. Biophys Acta 858 (1976) 161–168.
[34] D. Papahadjopoulos, K. Jacobson, S. Nir, T. Isac, Biochim. Biophys. Acta 311 (1973) 330–348.
[35] P. Van Hoogevest, J. De Gier, B. De Kruijff, FEBS Lett. 171 (1984) 160–164.
[36] E. Corvera, O.G. Mouritsen, M.A. Singer, M.J. Zuckermann, Biochim. Biophys. Acta 1107 (1992) 261–270.
[37] S.G. Clerc, T.E. Thompson, Biophys. J. 68 (1995) 2333–2341.
[38] T.-X. Xiang, B.D. Anderson, J. Pharm. Sci. 84 (1995) 1308–1315.
[39] T.-X. Xiang, B.D. Anderson, J. Membr. Biol. 148 (1995) 157–167.
[40] A.D. Bangham, M.M. Standish, J.C. Watkins, J. Mol. Biol. 13 (1965) 238–252.
[41] F. Olson, C.A. Hunt, F.C. Szoka, W.J. Vail, D. Papahadjopoulous, Biochim. Biophys. Acta 557 (1979) 9–23.
[42] J.R. Alger, J.H. Prestegard, Biophys. J. 28 (1979) 1–14.
[43] L.H. Piette, W.A. Anderson, J. Chem. Phys. 30 (1959) 899.
[44] T.-X. Xiang, X. Chen, B.D. Anderson, Biophys. J. 63 (1992) 78–88.
[45] T.-X. Xiang, B.D. Anderson, J. Pharm. Sci. 83 (1994) 1511–1518.
[46] S. Korman, V.K. LaMer, J. Amer. Chem. Soc. 58 (1936) 1396–1403.
[47] F. Snyder, in: D.E. Vance, J.E. Vance (Eds.), Biochemistry of Lipids and Membranes, Benjamin/Cummings, Menlo Park, CA, 1985, pp. 271–298.
[48] B.A. Cunningham, L. Midmore, O. Kucuk, L.J. Lis, M.P. Westerman, W. Bras, D.H. Wolfe, P.J. Quinn, S.B. Qadri, Biochim. Biophys. Acta 1233 (1995) 75–83.
[49] P. Laggner, K. Lohner, R. Koynova, B. Tenchov, Chem. Phys. Lipids 60 (1991) 153–161.
[50] R.N.A.H. Lewis, W. Pohle, R.N. McElhaney, Biophys. J. 70 (1996) 2736–2746.
[51] W.J. van Blitterswijk, B.W. van der Meer, H. Hilkmann, Biochemistry 26 (1987) 1746–1756.
[52] D.O. Shah, J.H. Schulman, J. Lipid Res. 8 (1967) 215–226.
[53] G.W. Stockton, I.C.P. Smith, Chem. Phys. Lipids 17 (1976) 251–263.
[54] T.-X. Xiang, B.D. Anderson, Biophys. J. 72 (1997) 223–237.
[55] J.H. Ipsen, O.G. Mouritsen, M.J. Zuckermann, Biophys. J. 56 (1989) 661–667.
[56] S. Mabrey, J.M. Sturtevant, Proc. Natl. Acad. Sci. U.S.A. 73 (1976) 3862–3866.
[57] M.B. Sankaram, T.E. Thompson, Proc. Natl. Acad. Sci. U.S.A. 88 (1991) 8686–8690.
[58] K. Mortensen, W. Pfeiffer, E. Sackmann, W. Kno, Biochim. Biophys. Acta 945 (1988) 221–245.
[59] R.P. Rand, V.A. Parsegian, J.A.C. Henry, L.J. Lis, M. McAlister, Can. J. Biochem. 58 (1980) 959–968.
[60] E.J. Shimshick, H.M. McConnell, Biochemistry 12 (1973) 2351.

[61] R.E. Jacobs, B.S. Hudson, H.C. Andersen, Biochemistry 16 (1977).
[62] J.A. Dix, D. Kivelson, J.A. Diamond, J. Membr. Biol. 40 (1978) 315–342.
[63] D. Bassolino-Klimas, H.E. Alper, T.R. Stouch, Biochemistry 32 (1993) 12624–12637.
[64] J.F. Nagle, H.L. Scott Jr., Biochim. Biophys. Acta 513 (1978) 236–243.
[65] C.D. Linden, K.L. Wright, H.M. McConnell, C.F. Fox, Proc. Natl. Acad. Sci. U.S.A. 73 (1973) 3862–3866.
[66] S. Doniach, J. Chem. Phys. 68 (1978) 4912–4916.
[67] M.I. Kanehisa, T.Y. Tsong, J. Am. Chem. Soc. 100 (1978) 424–432.
[68] M.L. Francoeur, G.M. Golden, R.O. Potts, Pharm. Res. 7 (1990) 621–627.
[69] S.W. Smith, B.D. Anderson, J. Pharm. Sci. 84 (1995) 551–556.
[70] P.F.F. Almeida, W.L.C. Vaz, T.E. Thompson, Biochemistry 31 (1992) 6739–6747.